Proceedings of the 11th ICPMG 2026
11th International Conference on Physical Modelling in Geotechnics
8-12 June 2026, Zurich, Switzerland

Comparison of THM-Controlled Centrifugal Model Tests and Numerical Simulations for Evaluating Long-Term Stability in HLW Geological Disposal

M. Sato
Central Research Institute of Electric Power Industry, Chiba, Japan, sato3763@criepi.denken.or.jp

M. Sawada, S. Nishimoto
Central Research Institute of Electric Power Industry, Chiba, Japan

ABSTRACT: For geological disposal of high-level radioactive waste (HLW), it is necessary to evaluate the long-term stability of the near field (the area surrounding the HLW disposal hole) following the emplacement of waste in deep underground bedrock. Therefore, attempts have been made to significantly shorten the time required for testing static physical phenomena using centrifugal model tests and to enhance the reliability of long-term near-field stability evaluations by comparing the results of centrifugal model tests with those of numerical models. However, controlling and measuring the heat, pore water, and stresses in scaled models of 1/30 or 1/50 used in centrifugal model tests tends to be technically challenging. In this study, we devised test vessels and scaled models to simulate heat generation from waste, and designed a test to obtain time-dependent changes in water infiltration and stress in the buffer material, enabling comparisons with thermal-hydraulic-mechanical simulations. Water tended to percolate from the outside to the vicinity of the heated overpack, and the numerical analysis reproduced the near-field behavior.

1 INTRODUCTION

The geological disposal of high-level radioactive waste (HLW) is planned to be carried out deep underground. The waste is sealed in a canister and enclosed in metallic casing (called an overpack). Subsequently, it is packed into a deposition hole drilled into the bedrock and surrounded by a bentonite buffer material. The area surrounding the HLW deposition hole (called the "near-field") is composed of such a heterogeneous composite. The long-term behavior in the near-field is governed by complex thermal, hydraulic, and mechanical (T-H-M) coupled processes that occur over 100 years and involve heat generation from the waste, groundwater infiltration, and the swelling pressure of the bentonite buffer (Figure 1). After resaturation, it is considered that the buffer will be secondarily consolidated owing to the weight of the overpack with the option of vertical emplacement in the buffer, and the overpack will gradually settle over a long period (Nakamura and Tanaka 2014; NUMO, 2021). Both full-scale tests and numerical simulations have been used to investigate the long-term behavior of the near-field. A previous study developed a T-H-M coupling code (LOSTUF; Numerical Code for LOng-term STability of Underground Facilities) to evaluate long-term behavior in the near-field (Sawada et al., 2006). However, when comparing the numerical simulation and data obtained for the full-scale test, validating and evaluating the behavior over 100 years proved challenging. One possible way to evaluate long-term behavior is through methods such as the centrifugal model test, which has the advantage of significantly shortening the time necessary to observe behavior resulting from typical groundwater flow according to the scaling law. A 1/N scale model in a centrifugal model test is subjected to N times the Earth's gravitational/centrifugal acceleration (G), and then, a centrifugal scaling law is applied in a static field, where N is the scale factor and gravity/centrifuge acceleration level (e.g., Taylor 1995; Kumar 2007). The scaling law is verified by the laboratory measurements of "modelling of models" at the several centrifugal force fields such as water migration in unsaturated soils (Thorel et al., 2002; Caiced and Thorel 2014) and heating migration in soils (Krishnaiah and Singh 2004). In light of this, some studies have also developed an accelerated test using a centrifuge to model long-term behavior in the HLW near-field (Nishimoto et al., 2011). Sawada et

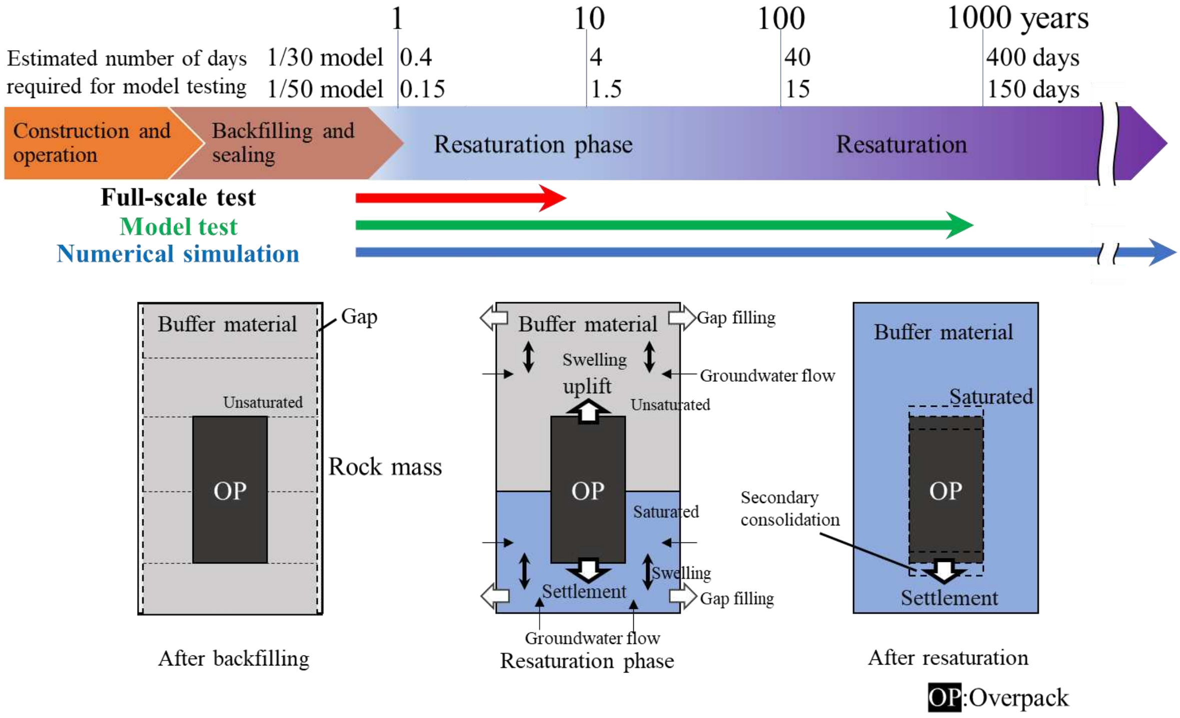

Figure 1. Image of near-field behavior during buffer resaturation process.

al. (2017) performed H-M-coupled numerical simulations of preliminary results from an H-M-coupled 1/30 scale model test (Nishimoto et al., 2016). However, because the permeability of the bentonite buffer is very low, it is difficult to secure enough time for sufficient evaluation until after resaturation using a 1/30 scale model test. In addition, the effects of waste heat were not considered in previous studies (Nishimoto et al., 2016). Therefore, to account for the effects of heat and conduct model tests in a shorter time, a small heater was used as model waste, and a 1/50 scale model was developed. The 1/50 scale is the minimum size at which the developed small heater, as well as water level sensors and soil pressure transducers, can be installed. When conducting a scaled-model test with a 1/50 scale model under 50 G acceleration, the scaling law provided an acceleration effect of 50^2 times, enabling the physical behavior equivalent to 273 years to be evaluated in 40 days of testing.

We evaluated near-field static behavior equivalent to 273 years in actual time by comparing scaled model tests and numerical simulations. Here, although the existence of fractures and heterogeneity in the buffer materials may result in deviations from strict similitude, these effects are assumed to be negligible in small scale models.

2 TEST CONDITIONS

2.1 Centrifuge equipment

We used “CENTURY5000-THM” (Centrifugal Test equipment for Ultralong time Range of 5000 years: simulating coupled T-H-M processes) (Nippon Steel & Sumikin Railway Technology Co., Ltd., special order) that enables us to perform a long-term operation of up to 6 months with a maximum payload of 1.5 ton up to 100 G (Nishimoto et al., 2011; 2016) (Figure 2). The greatest feature of this instrument is its capability for continuous operation for up to six months (whereas general centrifugal loading devices of a similar scale typically operate for only several tens of hours). In addition, because long-term operation is required, concrete pit houses require equipment with a large air-conditioning system that enables constant temperature control to prevent temperature rise resulting from air resistance. Furthermore, the main unit was equipped with a power supply system to counteract momentary power interruptions.

2.2 Scale model of near-field in the HLW disposal repository

In the overpack settlement analysis described in the Technical Report (NUMO 2021), the thickness of the

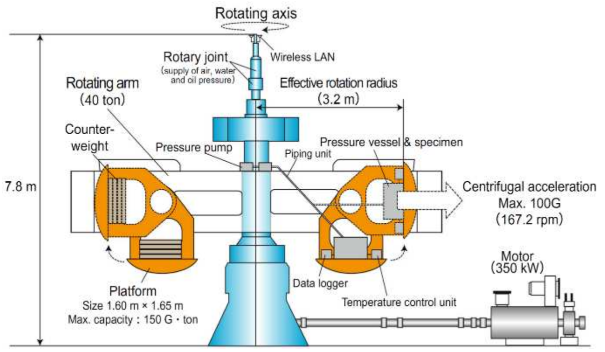

Figure 2. Schematic of the geotechnical centrifuge, CENTURY5000-THM (Nishimoto et al., 2016).

buffer was set to 700 mm with a sufficient margin to account for uncertainties, utilizing previous reports and referring to Ogata et al. (1999). We designed and created a new model with actual scales of 1/30 and 1/50, by referencing Ogata et al. (1999) (Figure 3). The 1/50 scale model of the compacted buffer had a diameter of 44.4 mm and a height of 82.6 mm. The scaled model was enclosed in an aluminum test vessel. The model overpack consisted of stainless steel (SUS316L) and epoxy resin. The 1/50 scale model of the overpack had a diameter of 16.4 mm and a height of 34.6 mm (Figure 4a). Assuming heat generation from waste, a heater was installed inside the overpack (Figure 4a). The heater wiring is designed to be accessible from the top of the test vessel. The weight of the overpack is adjusted using epoxy resin such that the bulk density becomes 6.35 Mg/m^3, based on the calculation of the weight and volume of the overpack, including vitrified waste. Six soil-pressure transducers and four water-level sensors were installed in the test vessel (Figure 3 and 4b). A gap sensor (noncontact displacement sensor) was installed at the bottom of the test vessel to measure the displacement (uplift and settlement) of the overpack by detecting changes in the distance to the target bar (rigidly connected to the model overpack). A gap sensor is an eddy-current sensor that generates a high-frequency magnetic field in the coil inside the sensor. It measures the distance to the target object by detecting voltage changes introduced by impedance variations according to the distance. The gap sensor can gauge the uplift of the model overpack up to a maximum of 2.5 mm (equivalent to 75 mm on an actual scale).

The buffer was prepared by compacting Japanese Ca-bentonite powder (Kunibond). An effective montmorillonite dry density (ρ_{em}: representing bulk density when the specimen is composed of only montmorillonite) of compacted buffer was 1.0 Mg/m^3.

$$\rho_{em} = \frac{m_m}{V_a+V_w+V_m} \quad (1)$$

where, m_m is the mass of montmorillonite (Mg), V_a, V_w, and V_m are the volumes of air, water, and montmorillonite (m^3), respectively. The montmorillonite content was determined by measuring the methylene blue adsorption amount in accordance. The methylene blue adsorption amount of Kunibond was 122 mmol/100 g, assuming that the methylene blue adsorption amount of the

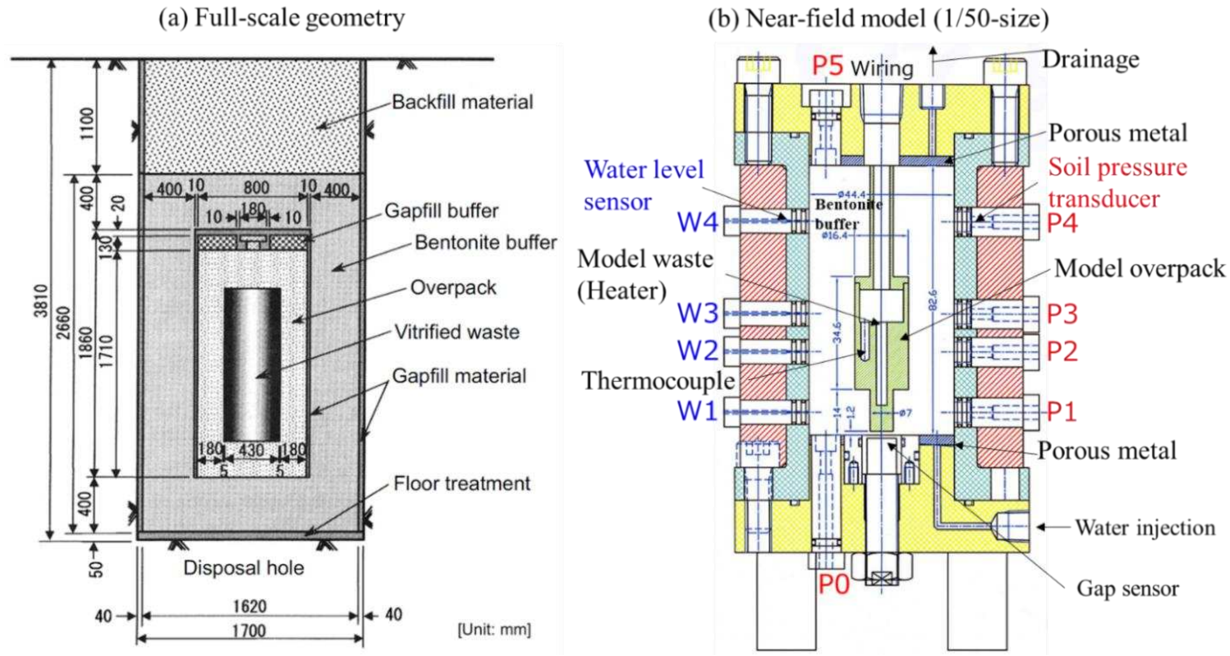

Figure 3. (a) The target HLW disposal repository (Ogata et al., 1999) and (b) the Near-field model of the centrifugal 1/50 scaled model test.

montmorillonite contained in Kunibond was 150 mmol/100 g (Watanabe & Yokoyama, 2020).

2.3 Test cases

The centrifugal model tests were conducted using 1/30 and 1/50 scale model (Table 1). The temperature of the model waste was set to 90 °C. Even under the 90 °C model waste condition, the outside of the test vessel was kept constantly at room temperature (25 °C) by the apparatus, resulting in a temperature gradient from the model waste to the outside of the test vessel. The test water injection pressure was set at 1.0 MPa, and the test water was injected from the bottom of the test vessel. Assuming coastal geological disposal of HLW (NUMO 2021), artificial seawater (Marine Art SF-1, Osaka Yakken) was used as test water.

Table 1. Cases of the centrifugal model tests

cases	heat	scale	test days	years in actual scale
Case 1	90 °C	1/30	43	105
Case 2	90 °C	1/50	40	273

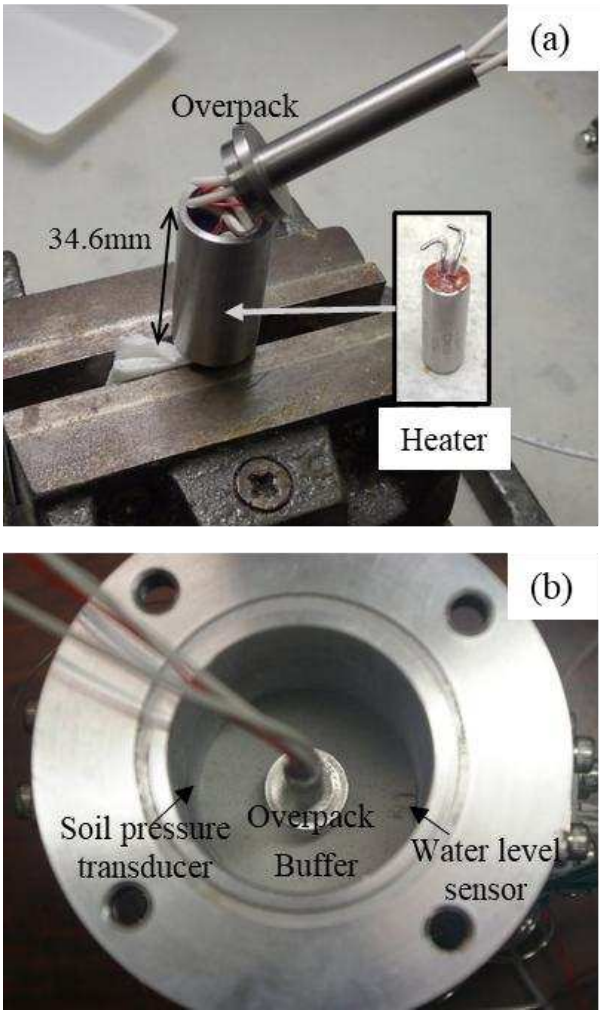

Figure 4. Assemblies of the 1/50 scaled model test.

3 NUMERICAL SIMULATION

3.1 T-H-M-Coupled formulation by LOSTUF

The original formulation of coupled hydroelasticity was extended to a partially saturated thermohydroelastic medium (Sawada et al., 2006). Three phases are considered in this formulation: solid, liquid, and gas. However, the gas pressure is assumed to be constant and equal to atmospheric pressure throughout the porous medium. Vapor transport occurs only through molecular diffusion driven by a gradient in the vapor concentration (Fick's law), whereas the advection of vapor with the bulk gas flow is neglected. LOSTUF adopts a compositional approach to establish mass balance equations. This approach entails balancing the species rather than the phases. Balance equations are considered for the energy, water mass, and momentum. The final governing equations in terms of the displacement vector $\boldsymbol{u}$, pore pressure P, and absolute temperature T are obtained by substituting constitutive laws, including Darcy's, Fick's, and Fourier's laws, into the balance equations.

The governing equation for water flow is obtained as

$$\rho_l S_l \frac{\partial(\nabla\cdot\boldsymbol{u})}{\partial t} + [\rho_{l0}\phi S_l \beta_{Pl} + (\rho_l - \rho_v)C_{lP} + \rho_l C_{vP}]\frac{\partial P}{\partial t} - (\rho_{l0}\phi S_l \beta_{Tl} - \rho_l C_{vT})\frac{\partial T}{\partial t} + \nabla\cdot [-\rho_l \frac{\boldsymbol{k}k_{rl}}{\mu_l} - \rho_l D_{Pv}\boldsymbol{I})\nabla P] + \nabla\cdot[(-\rho_l D_{Tv})\boldsymbol{I}\nabla T] = Q_B + \nabla\cdot(\rho_l \frac{\boldsymbol{k}k_{rl}}{\mu_l}\boldsymbol{g}) \tag{2}$$

where ρ_l is the liquid water density, ρ_{l0} is the reference liquid water density, ρ_v is the vapor water density, S_l is the liquid water saturation, and ϕ is the porosity. β_{Pl} is the compressibility of water, β_{Tl} is the linear thermal expansion coefficient of water, $\boldsymbol{k}$ is the intrinsic permeability tensor, k_{rl} is the relative permeability function, μ_l is the fluid viscosity, $\boldsymbol{I}$ is the identity tensor, Q_B is the source term of the water flow, and $\boldsymbol{g}$ is the gravity acceleration vector. C_{lP} is the liquid water capacity obtained from the water retention curve. C_{vT} is the thermal vapor water capacity at a constant temperature and D_{Pv} and D_{Tv} are the isothermal and thermal vapor diffusion coefficients, respectively, as follows:

$$D_{Pv} = \frac{D_v \rho_v}{\rho_l^2 R_v T} \tag{3a}$$

$$D_{Tv} = D_v\left(\frac{RH}{\rho_l}\frac{\partial \rho_{vS}}{\partial T} - \frac{\rho_v P_l}{\rho_l^2 R_v T^2}\right) \tag{3b}$$

where, RH is the relative humidity, R_v is the specific gas constant of the water vapor [=461.5 J/(kgK)], ρ_{vS} is the saturated vapor density which is dependent on the temperature. D_v is the molecular diffusion coefficient of water vapor and is defined as

$$D_v = \phi(1 - S_l)\tau D_m \quad (4)$$

where, τ is the tortuosity factor and D_m is the molecular diffusion coefficient for the vapor flow in air.

The governing equation for the heat transfer is obtained as

$$(1-\phi)3K_D\beta_{TD}T\frac{\partial(\nabla\cdot\boldsymbol{u})}{\partial t} + (\rho c)_m\frac{\partial T}{\partial t} - \nabla\cdot \left[T\left(\frac{\beta_{Tl}}{\beta_{Pl}}\right)\frac{\boldsymbol{k}k_{rl}}{\mu_l} + \rho_l L D_{Pv}\boldsymbol{I}\right]\nabla P - \nabla\cdot(\lambda_m\boldsymbol{I}\nabla T) + (c_l\boldsymbol{q}_l)\cdot\nabla T = Q_{TB} \quad (5)$$

where, K_D is the bulk modulus of the solid phase, β_{TD} is the drained linear thermal expansion coefficient of the medium, L is the latent heat of vaporization of water, Q_{TB} is a heat-source term, λ_m is the thermal conductivity of the medium, and $(\rho c)_m$ is the heat capacity of the unit volume of medium.

For the stress equilibrium, the governing equation is as follows:

$$\nabla\cdot\left[\boldsymbol{D}:\frac{\partial(\nabla\boldsymbol{u}+(\nabla\boldsymbol{u})^{tr})}{\partial t}\right] + \nabla\cdot\left(-\boldsymbol{I}\chi\frac{\partial P}{\partial t}\right) + \nabla\cdot \left[(-\boldsymbol{D}:\boldsymbol{I}\beta_{TD})\frac{\partial T}{\partial t}\right] = \frac{\partial}{\partial t}(\rho_m\boldsymbol{g}) + \boldsymbol{F}_B + \boldsymbol{F}_P \quad (6)$$

where, $\boldsymbol{D}$ is the tangential stiffness tensor for the solid phase, and it can be defined by Young's modulus E and Poisson's ratio υ for a linear isotropic elastic body. χ is Bishop's parameter for effective stress, and $\chi = 0$ for unsaturated media. ρ_m is the density of the mixture, and $\boldsymbol{F}_B$ is an external force vector. $\boldsymbol{F}_P$ is a nodal force vector generated by swelling as follows:

$$\boldsymbol{F}_P = \int \boldsymbol{B}^T\boldsymbol{D}(\omega_{smax} - \varepsilon_{aw})\boldsymbol{I}dV \quad (7)$$

where, $\mathbf{B}$ is the strain-displacement operator matrix, and ε_{aw} is the accumulated swelling strain. The maximum swelling strain at an unsaturated state ω_{smax} is determined by the following equation (Komine and Ogata 2003) obtained from Kunigel V1 (Japanese Na-bentonite).

$$\omega_{smax} = \varepsilon_{smax}\left(\frac{|P_l - P_{l0}|}{|P_{l0}|}\right)^l \quad (8)$$

where, ε_{smax} is the maximum swelling strain during swelling test.

3.2 Basic assumptions and boundary conditions

The simulation focused on water flow in the buffer and the mechanical behavior of the buffer and overpack within a cylindrical vessel. The simulation model was assumed to be axisymmetric. Joint elements were set at the boundaries between the buffer and vessel as well as between the buffer and model overpack. For the hydraulic boundary conditions, a water injection pressure of 1.0 MPa was applied to the bottom surface of the buffer material and drained from the top surface of the buffer. The outer surface was set as a nondrainage boundary. For the thermal boundary conditions in the case without heating, all nodes were fixed at 25°C. In the case with heating, the temperature of the model overpack was raised to 90°C and the outer boundary to 30°C over 1.5 months, and then both were kept constant based on centrifugal motel test results.

3.3 Material properties

Table 2 lists the material properties used in the simulations. The constitutive equation for the buffer was an elastic model, and the relationship between the Young's modulus E_{50} (MPa) and the saturation degree (%) was applied following the equation based on the test results using Kunigel V1 and deionized water (Sawada et al., 2023).

$$E_{50} = 171 - 1.41S_l \ (E_{50} \geq 10\ MPa) \quad (9)$$

$$\upsilon = 0.30 + 0.0019S_l \quad (10)$$

The swelling characteristics were organized based on the relation between the effective clay density ρ_c (Mg/m^3) and the equilibrium swelling pressure P_s (MPa) at saturation. Parameters p and q were set accordingly (Figure 5).

$$P_s = p\cdot exp\,(q\cdot\rho_c) \quad (11)$$

Soil water characteristic curve was set using van Genuchten equation.

$$S_l = S_{l0} + (S_{lmax} - S_{l0})\left[1 + \left(\frac{s}{P_0}\right)^{\frac{1}{1-\lambda}}\right]^{-\lambda} \quad (12)$$

where s is the suction, P_0 is the suction parameter that determines the soil–water characteristic curve, $S_{l0} = 0.1$ and $S_{lmax} = 1.0$. The initial suction was set to 55 MPa for all cases, as described in a previous study (Sawada et al., 2023). The hydraulic conductivity k_w (m/s) was defined as a function of ρ_c (Mg/m^3), and parameters a and b were determined from laboratory test results (Figure 5).

$$k_w = a\cdot exp\,(b\cdot\rho_c) \quad (13)$$

The thermal conductivity λ_m was defined as a function of the saturation degree.

$$\lambda_m = (1 - S_l)\lambda_{dry} + S_l\lambda_{sat} \quad (14)$$

where, λ_{dry} is dry thermal conductivity and λ_{sat} saturated thermal conductivity. The specific heat c_s (J/kgK) of the Kunibond was defined as a function of the temperature T (°C).

$$c_s = 1.5T + 811 \quad (15)$$

The centrifugal model tests were conducted for a period equivalent to 273 years on an actual scale, whereas the numerical simulations were conducted for up to 1000 years to assume complete saturation.

Table 2. Material properties

Bentonite	Kunibond
Effective dry density	1.12 Mg/m^3
Montmorillonite content percentage	81.3 %
Effective montmorillonite dry density	1.0 Mg/m^3
Skeletal density	2.67 Mg/m^3
Young's modulus	*eq.* (9)
Poisson's ratio	*eq.* (10)
Swelling characteristic parameter $\boldsymbol{p}$	1.21x10^{-3} MPa
Swelling characteristic parameter $\boldsymbol{q}$	5.49
Soil water characteristic curve $\boldsymbol{P_0}$	5.2 Mpa
Soil water characteristic curve $\boldsymbol{\lambda}$	0.35
Hydraulic parameter $\boldsymbol{a}$	1.59x10^{-5} m/s
Hydraulic parameter $\boldsymbol{b}$	-14.6
Dry thermal conductivity $\boldsymbol{\lambda_{dry}}$	0.300
Saturated thermal conductivity $\boldsymbol{\lambda_{sat}}$	1.300
Specific heat of solid	*eq.* (14)
Linear thermal expansion coefficient	1.16x10^{-3} K^{-1}

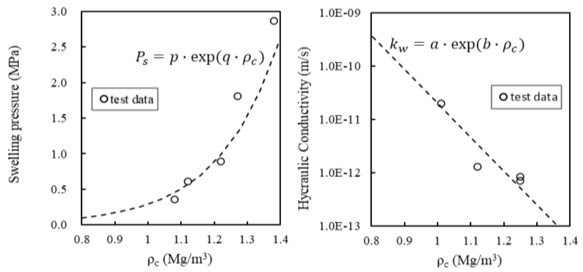

Figure 5. Relationship between P_s and k_w as a function of ρ_c

4 RESULTS

Figure 6 shows the saturation distribution for Case 2 of the centrifugal model test (a) and numerical simulation (b). In Figure 6(a), the buffer is considered to be nearly saturated when the output voltage reaches 3 V, based on the settings of the function generator. The buffer was saturated slightly earlier in the simulation than in the model test; however, the degree of saturation that increased sequentially from the bottom of the buffer was consistent in both cases. Figure 7 shows the soil pressure distribution for Case 2 of the centrifugal model test (a) and numerical simulation (b). In the simulation, the soil pressure exhibited complex behavior; however, after saturation, the soil pressure converged to a constant value. However, in the model test, it took longer for the soil pressure to converge, and the absolute values of the soil pressure distribution after 273 years on the actual scale were considered to exhibit a similar trend to those in the simulation.

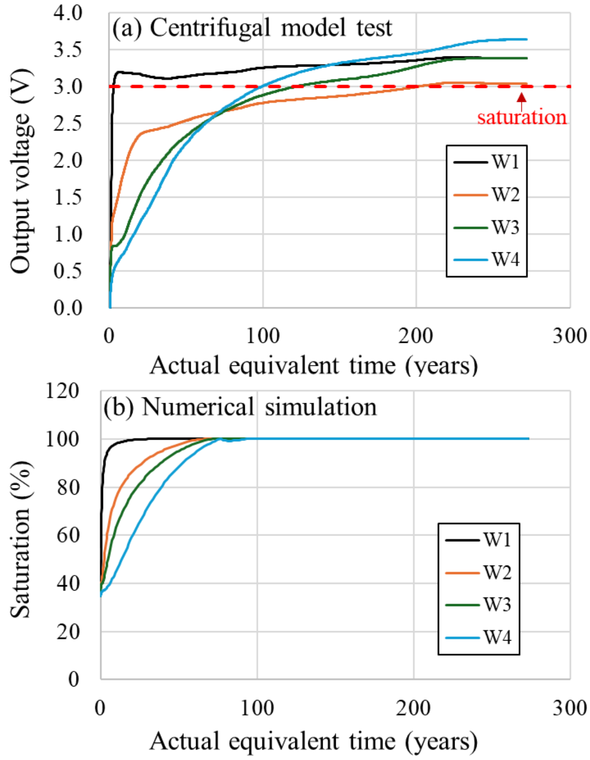

Figure 6. The saturation distribution

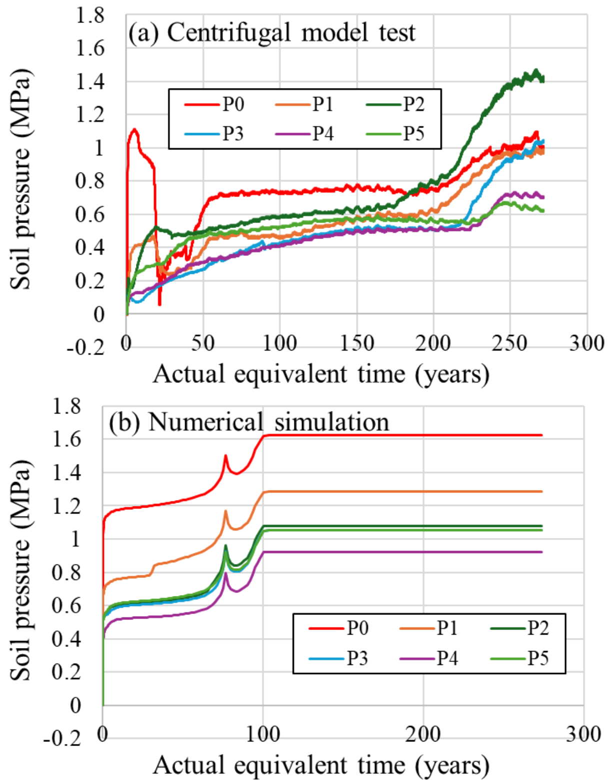

Figure 7. The soil pressure distribution

Figure 8 shows the displacement of the model overpack in Cases 1 and 2 of the centrifugal model test and simulation. The overpack displacement exhibited complex behaviors, such as uplift, settlement, and uplift movement. Although there were differences in timing and values between the simulation and model tests, complex displacements were observed in both cases. These results are attributed to changes in the swelling behavior.

Figure 9 shows the cross-sectional photographs and X-ray CT images taken after the centrifugal model tests. The initial density of the buffer material shown in the CT images was 1.12 Mg/m³, increasing to 2.12 Mg/m³ upon saturation. In Case 1, the test was completed after 105 years, and the results revealed regions with low saturation distributed along the sides and top of the model overpack. This distribution is attributed to the diffusion of water vapor caused by the temperature gradient, which generates a flow of water vapor from the model overpack toward the outside. In contrast, Case 2 exhibited uniform CT values, indicating that the buffer was saturated. Figure 10 shows the distributions of the water content and temperature obtained from the simulation. Although the buffering was slightly faster in the simulation than in the model test, the process progressed from the outside to the vicinity of the overpack. The results of the T-H-M model test and simulation confirmed a tendency for fluid to permeate by bypassing the area around the overpack. However, from a comprehensive assessment of the results, it was observed that soil pressure and overpack displacement converged earlier in the numerical simulations than in the model tests. One contributing factor may be the difference in water infiltration rates between the model experiments and the numerical simulations, potentially caused by an overestimation of hydraulic conductivity and young's modulus. Furthermore, the discrepancy between the idealized homogeneous conditions in the numerical model and the microscopic heterogeneity of the model is identified as a subject for future investigation.

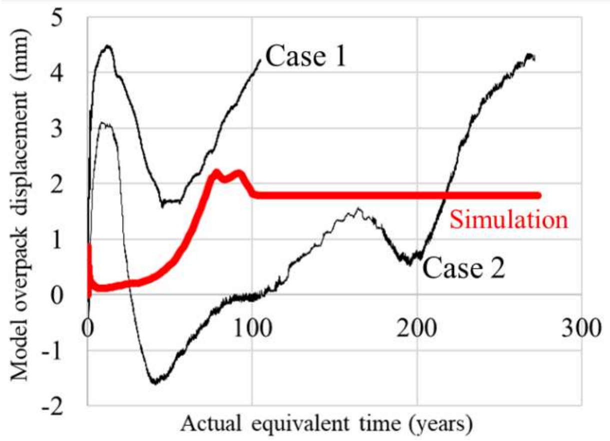

Figure 8. The displacement of overpack

5 CONCLUSIONS

In this study, to address the need for long-term behavior evaluation of HLW, small-scale assemblies with 1/50 size that allow heating of model waste up to 90 °C were developed, and centrifugal model tests and THM-coupled simulation were conducted. Both the test and simulation confirmed that the water flow in the buffer was affected by heat from the model waste. Although the overpack exhibited complex displacement influenced by the behavior of the buffer material under the present conditions, the displacement magnitude was very small, on the order of a few millimeters at the actual scale. Estimating the displacement behavior of the overpack enables

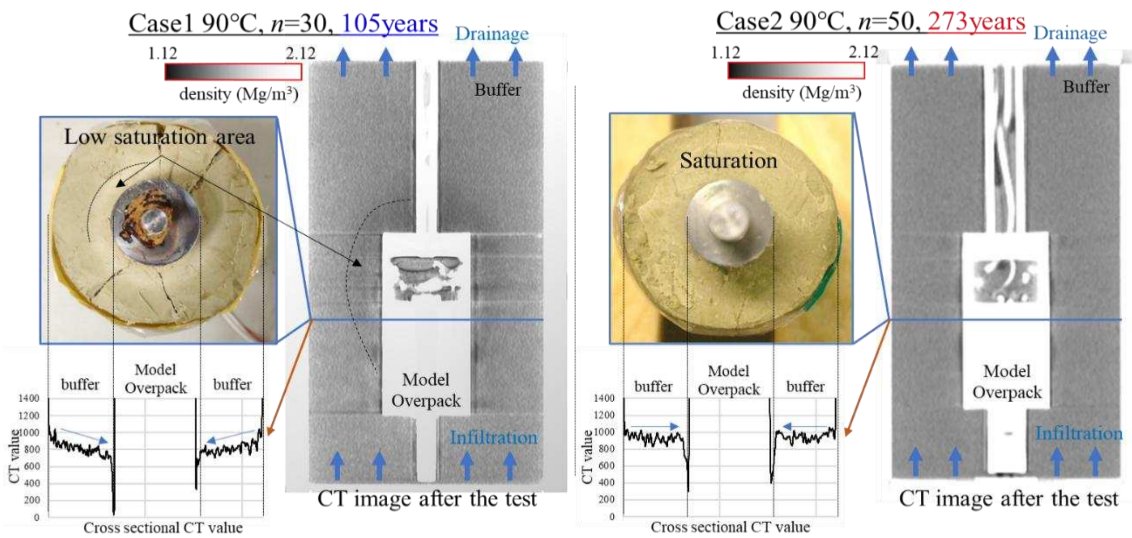

Figure 9. Cross-sectional photographs and X-ray CT images taken after the centrifugal model tests

feedback to the construction conditions of geological disposal. We will proceed with the appropriate acquisition of the material properties and future parameter studies.

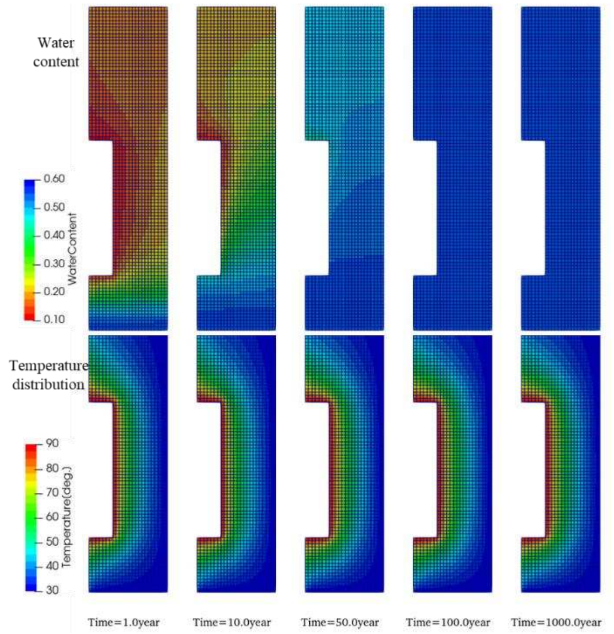

Figure 10. Distributions of water content and temperature.

ACKNOWLEDGEMENTS

This study was carried out under a contract with the Ministry of Economy, Trade and Industry (METI) as part of its R&D supporting program titled " The project for validating assessment methodology of geological disposal system in coastal region" Grant Number JPJ007597.

REFERENCES

Caiced, B. and Thorel, L. (2014). Centrifuge modelling of unsaturated soils. *Journal of Geo-Engineering Sciences*, 2(83-103). https://doi.org/10.3233/JGS-130013

Komine, H. and Ogata, N. (2003). New equations for swelling characteristics of bentonite-based buffer materials. *Canadian Geotechnical Journal*, 40:460–475. https://doi.org/10.1139/t02-115

Krishnaiah, S. and Singh, D. N. (2004). Centrifuge modelling of heat migration in soils. *International Journal of Physical Modelling in Geotechnics*. 4(3):39-47. https://doi.org/10.1680/ijpmg.2004.040303

Kumar, P. (2007). Scaling Laws and Experimental Modelling of Contaminant Transport Mechanism through Soils in a Geotechnical Centrifuge. *Geotechnical and Geological Engineering*, 25:581–590. https://doi.org/10.1007/s10706-007-9131-x

Nishimoto, S., Okada, T. and Sawada, M. (2011). Simulation of ultra-long term behavior in HLW near-field by centrifugal model test (part 1)—development of centrifugal equipment and centrifuge model test method—. CRIEPI Res. Rep. N10018 (in Japanese with English abstract)

Nishimoto S, Sawada M, Okada T (2016) New rapid evaluation for long-term behavior in deep geological repository by geotechnical centrifuge. Part 1: test of physical modeling in near-field under isotropic stress-constrain conditions. *Rock Mechanics Rock Engineering*. 49:3323-3341. http://doi.org/10.1007/s00603-016-0972-6

Nuclear Waste Management Organization of Japan, NUMO. (2021). The NUMO pre-siting SDM-based safety case. NUMO-TR-21-01.

Ogata, N., Kosaki, A., Ueda, H., Asano, H. and Takao, H. (1999). Execution techniques for high level radioactive waste disposal: IV. Design and manufacturing procedure of engineered barriers. *Journal of Nuclear Fuel Cycle and Environment*, 5:103–121. https://doi.org/10.3327/jnuce.5.103

Sawada, M., Nishimoto, S. and Okada, T. (2017). New rapid evaluation for long-term behavior in deep geological repository by geotechnical centrifuge—Part 2: Numerical simulation of model tests in isothermal condition. *Rock Mechanics Rock Engineering*, 50:159-169. http://doi.org/10.1007/s00603-016-1061-6

Sawada, M., Okada, T. and Hasegawa, T. (2006) Development of a numerical code for the prediction for the long-term behavior of the underground facilities for the high-level radioactive waste disposal. CRIEPI Res. Rep. N05028 (in Japanese with English abstract).

Sawada, M., Sato, M. and Nishimoto, S. (2023). Numerical analysis of re-saturation of buffer material and overpack displacement behavior in saltwater environment. *Proceedings of the 49th Symposium on Rock Mechanics*. 259-264. (in Japanese)

Taylor, R. N. (1995): Geotechnical centrifuge technology. Lackie Academic and Professional, London.

Thorel, L., Favraud, C. and Garnier, J. (2002). Mariotte bottle in a centrifuge: a device for constant water table level. *International Journal of Physical Modelling in Geotechnics*, 2(1):23-26. https://doi.org/10.1680/ijpmg.2002.020103

Watanabe, Y. and Yokoyama, S. (2020). Evaluation of montmorillonite content of bentonite considering accuracy of methylene blue adsorption test. *Journal of JSCE*, 76:26-39. (in Japanese with English abstract). https://doi.org/10.2208/jscejge.76.1_26